HHS Public Access

Author manuscript

*Nanoscale*. Author manuscript; available in PMC 2016 April 28.

Published in final edited form as:

*Nanoscale*. 2015 April 28; 7(16): 7115–7126. doi:10.1039/c4nr06164k.

# Nanoscale materials for hyperthermal theranostics

**Bennett E. Smith**[a], **Paden B. Roder**[b], **Xuezhe Zhou**[b], and **Peter J. Pauzauskie**[*,b,c]

[a] Department of Chemistry, University of Washington, Seattle, Washington

[b] Material Science & Engineering Department, University of Washington, Seattle, Washington

[c] Fundamental & Computational Sciences Directorate, Pacific Northwest National Laboratory, Richland, Washington

## Abstract

Recently, the use of nanoscale materials has attracted considerable attention with the aim of designing personalized therapeutic approaches that can enhance both spatial and temporal control over drug release, permeability, and uptake. Potential benefits to patients include the reduction of overall drug dosages, enabling the parallel delivery of different pharmaceuticals, and the possibility of enabling additional functionalities such as hyperthermia or deep-tissue imaging (LIF, PET, etc.) that complement and extend the efficacy of traditional chemotherapy and surgery. This mini-review is focused on an emerging class of nanometer-scale materials that can be used both to heat malignant tissue to reduce angiogenesis and DNA-repair while simultaneously offering complementary imaging capabilities based on radioemission, optical fluorescence, magnetic resonance, and photoacoustic methods.

## Introduction

Despite decades of research and development into small-molecule pharmaceuticals and advanced surgical methods, cancer remains one of the leading causes of death in industrialized societies[1]. Hyperthermal treatment is advantageous due to the reduced heat tolerance of cancer cells and dates as far back as 1600 BCE when tumors in breast tissue were treated with cauterization using a hot firedrill[2]. Non-contact methods of heating tumors have received much attention among researchers recently and include microwaves[3], radiofrequency[4], and ultrasound waves[5]. Photothermal therapy (PTT) uses light in the visible or near-infrared region of the spectrum as an energy source and would not have acheived the same success without the advent of the laser[6]. The massive electric fields induced by a laser can certainly heat cancer tissues through natural chromophore absorption, however their low absorption cross section makes it difficult to localize heat generation[7]. Dye molecules with greater absorption can be introduced into tumors but they often suffer from photobleaching and can diffuse out of the tumor into the healthy, surrounding tissue[8,9]. Nanoscale materials are known to exhibit a range of unique physical and chemical properties such as tunable sizes, high surface areas (~1000 $m^2/g$), biocompatibility, singlet oxygen generation, and large optical absorption coefficients that have led many researchers across

*peterpz@u.washington.edu.

the globe to consider them in next-generation PTT clinical trials. Hybrid nanomaterials, including gold-polymer structures, have also shown the ability to release a payload of chemotherapeutic small molecules due to volumetric contraction following photothermal heating[1].

This mini-review is focused on the fundamental physical processes that enable hyperthermal heating of several metallic, semiconducting, and insulating classes of nanomaterials, followed by recent results from in vitro or in vivo trials. Synergistic applications between hyperthermal heating and other diagnostic or therapeutic capabilities are highlighted at the end of each section to provide a sense of the multimodal therapeutic and diagnostic (theranostic) potential for these engineered nanomaterials.

## Heat equation

The temperature distribution around a heated nanoscale particle can be modelled using the following differential equation, regardless of the composition or morphology of the nanostructure being investigated:

$$\rho C_p \frac{\partial T}{\partial t} = \kappa \nabla^2 T + Q(\mathbf{r}, t) \quad (1)$$

where **r** and $t$ represent spatial coordinates and time, respectively, $T$ is the temperature, and ρ, $C_p$, and κ are the density, specific heat, and thermal conductivity of the material, respectively. $\rho C_p \frac{\partial T}{\partial t}$ represents the time-dependent increase of thermal energy within the nanostructure, $\kappa \nabla^2 T$ represents the diffusion of heat within the material (with an assumption of isotropic thermal conductivity), and $Q(\mathbf{r},t)$ represents a volumetric generation of heat energy within the material that depends on the composition and physical mechanism for heat generation. With appropriate boundary conditions based on morphology and an expression for the magnitude of $Q(\mathbf{r}, t)$, analytical predictions of steady-state temperature can be developed for any nanostructure. The next sections of this review discuss photothermal[10] generation of heat within metallic (i.e., gold) and semiconducting (i.e., silicon) materials, including carbon nanotubes, in addition to the inductive generation of heat within biocompatible ferrimagnetic materials (including $Fe_3O_4$) through the use of an AC-magnetic field.

## Gold Nanocrystals

Metallic nanomaterials including gold and silver nanocrystals[11,12] and nanorods[13] have been shown to generate localized hyperthermal heating through the absorption of incident optical radiation and surface plasmon relaxation[14–16]. Heating of gold nanoparticles has also been demonstrated under radiofrequency (RF) fields[17]; however, multiple heating mechanisms have been proposed and the degree to which the gold particles heat in the RF field is uncertain[18]. For optical fields, if the wavelength of light is resonant with the frequency of the surface plasmon for a given nanostructure, then the collective excitation of electrons (plasmons) can lead to large internal heating of the metallic nanostructure[15]. The lattice of metal atoms within the nanocrystal experiences heating following plasmon excitation through electron-phonon scattering on the timescale of 3 ps[19]. Plasmon resonance frequencies for a particular nanostructure depend on morphology and dielectric environment

and determination of resonance wavelengths is generally done via absorption spectroscopy[15,20,21].

In particular, spherical gold nanocrystals (AuNCs) have been studied extensively for their plasmonic potential[11,14,15,22–24]. Laser heating of AuNCs has been modeled theoretically with a source function that depends on both the dielectric functions of the metal/surroundings, and also local electric fields within the particle[11]:

$$\begin{aligned} Q(\mathbf{r},t) &= \langle \mathbf{j}(\mathbf{r},t)\cdot\mathbf{E}(\mathbf{r},t)\rangle \\ &= -\tfrac{1}{2}Re\left[i\omega\tfrac{\varepsilon(\mathbf{r})-1}{4\pi}\tilde{\mathbf{E}}(\mathbf{r})\tilde{\mathbf{E}}^{*}(\mathbf{r})\right] \end{aligned} \quad (2)$$

where $\mathbf{j}(\mathbf{r},t)$ is the electric current density, $\mathbf{E}(\mathbf{r},t) = \mathrm{Re}[\tilde{\mathbf{E}}(\mathbf{r})e^{(-i\omega t)}]$ is the resulting electric field in the system, $\varepsilon(\mathbf{r})$ is the dielectric constant for the metal, and $\tilde{\mathbf{E}}(\mathbf{r})$ and $\tilde{\mathbf{E}}^{*}(\mathbf{r})$ are the complex electric field and its complex conjugate, respectively.

The solution to equation (1) with the source term given in equation (2) was obtained by Govorov et al.[11] for the steady state ($t \to \infty$). They found that the generated surface plasmons result in temperature maxima at the surface ($r = R$) of these materials which is given by[15]:

$$\Delta T_{max}(I_0) = \frac{R^2}{3\kappa_0}\frac{\omega}{8\pi}\left|\frac{3\varepsilon_0}{2\varepsilon_0+\varepsilon}\right| Im\varepsilon\frac{8\pi I_0}{c\sqrt{\varepsilon_0}} \quad (3)$$

where $I_0$ is the irradiance in the surrounding medium, $\kappa_0$ and $\varepsilon_0$ are the thermal conductivity and dielectric constant, respectively, of the surrounding medium, and $c$ is the speed of light in vacuum. A sample calculation shows that for an AuNP with a 100 nm radius, an irradiance of 1 kW/cm$^2$ would give a temperature increase of ~ 5°C[15]. For metallic (i.e., plasmonic) particles in general, the recently developed thermal discrete dipole approximation (t-DDA) code[25] provides a method for determining the steady-state temperature within the particles and in homogeneous, surrounding medium.

The localized surface plasmon resonance (LSPR) and, consequently, the heating efficiency will depend significantly on the particles' composition and geometry. For example, spherical AuNCs with diameters between 10 nm and 100 nm exhibit resonances ranging from 517 nm to 575 nm[23]. However, tissue absorption at visible wavelengths limits the application of noble metal nanoparticles as an in vivo photothermal therapy. To achieve efficient heating at depths greater than 3 cm, the nanoparticles' size and shape need to be engineered to shift the LSPR into the near infrared (NIR) tissue-transparency window (~800 nm)[26–29]. The ability to tune gold nanoparticles' LSPR was pioneered by Catherine Murphy using the seed-mediated method to grow nanorods[30] and sees benefits in imaging[21,31–33], diagnosis[34,35], photothermal therapy[13,26,32,36–40], and drug delivery[41–46].

In vivo NIR PTT has already been shown using colloidal gold nanorods (AuNRs) with an optimized longitudinal plasmon. Dickerson et al.[26] demonstrated a substantial decrease in size for squamous cell carcinoma xenografts for pegylated AuNRs for both direct injections as well as intravenous injections. Wu et al.[36] also showed the high spatial precision regioselectivity of this therapy. Their experiments used an 800 nm femtosecond pulsed laser

to irradiate human liver cancer cells with internalized AuNRs. They show localized cell necrosis after laser irradiation while cells a few hundred microns away from the laser spot were unaffected and cells alone (without internalized AuNRs) were undamaged by direct laser exposure.

PTT also has the potential to treat multidrug-resistant (MDR) bacteria. By covalently conjugating gold nanorods to antibodies specific to Pseudomonas aeruginosa, one of the leading causes of increased infection and mortality rate among individuals with weakened immune systems, Norman et al.[47] were able to significantly reduce the bacterial cell viability using a 785 nm light source.

In addition to preventing angiogenesis with tumors and treating bacterial infections, the identification of diseased tissues is also crucial for effective treatment of metastatic tumors. This need for biomedical imaging has stimulated additional interest in designing gold[33] and hybrid[48] nanomaterials that can be used for both photothermal heating and optical or gamma-ray imaging[33]. Imaging of these tissues was demonstrated by two-photon excitation of endogenous fluorophores at depths up to 40 $\mu$m[49]. However, optical contrast agents including semiconductor[50] and noble metal[51] particles targeted for biomolecular signatures can be used to confirm cancerous tissues more definitively. Although semiconductor quantum dots have shown a two-photon cross section at least 30 times greater than the organic fluorophores, they are generally unsuitable for clinical application due to their heavy metal composition[52]. Noble metals like gold are biocompatible and show an increase in two-photon cross sections over organic fluorophores by at least one order of magnitude.

The targeting of small-molecule pharmaceuticals to specific sites often requires direct injection at the site; otherwise drugs are delivered through methods (i.e. orally, intravenously) that expose multiple organ systems and may have adverse side effects. The use of nanoparticles (NPs) in drug delivery can allow for externally stimulated triggered-release of molecules through a variety of methods. Angelatos et al.[53] have demonstrated a facile route for macromolecule encapsulation and release where multi-layered polyelectrolyte microcapsules are used to entrap the specific molecule and then dotted with AuNCs. Upon NIR irradiation, the microcapsules shells disintegrated as a result of the photothermal heating of the AuNPs. They further showed that active targeting of the microcapsules is achieved through surface functionalization. One problem with drug delivery is heterogeneity within the tumor due to irregular blood vessel architecture, elevated interstitial fluid pressure from poor lymphatic drainage, and hindered diffusion from a dense intercellular matrix[54]. Gormley et al.[37] were able to demonstrate the benefit of plasmonic photothermal therapy for increasing the overall accumulation and penetration of N-(2-hydroxypropyl)methacrylimide (HPMA) within a prostate tumour using AuNRs and 808 nm laser light (Fig. 1).

The plasmonic properties of AuNCs have also found use in other therapies including photodynamic therapy (PDT). During PDT, oxygen molecules in the tissue are excited from a relatively inert triplet ground-state ($^3O_2$) to a highly reactive excited singlet state ($^1O_2$) through direct energy transfer or electron exchange with a photosensitizing molecule. High electric fields from surface plasmons can enhance the absorption and, therefore, generation

of singlet-oxygen from small molecule photosensitizers[31,44]. More recently, AuNCs *themselves* have even been shown to act as photosensitizers directly[55,56] through a proposed hot-electron ejection[20] mechanism.

## Semiconductor Nanostructures

Semiconducting nanomaterials have also received a significant amount of recent attention for hyperthermal theranostics. However, in contrast to metallic nanostructures, semiconductors can be photothermally heated through the excitation of direct (band-to-band) transitions, indirect transitions, and also plasmonic photoexcitation. LSPRs have recently been shown to exist in many semiconducting nanomaterials arising from appreciable free carrier concentrations, which are easily controlled though doping and tunable from around $10^{16} – 10^{21}$ $cm^{-3}$ (Ref. [57]). The doping is achieved through either intrinsic defects (such as copper deficiencies in copper chalcogenides[58–60] and oxygen deficiencies in transition-metal oxides[61,62]) or the addition of extrinsic impurities[63,64]. Moreover, while the NIR absorption of metallic NPs is largely due to their LSPR, NIR absorption in semiconductors is a combined consequence of their LSPR as well as band-to-band transition of the charge carrier. This property allows tunability of the NIR absorption of nanoscale semiconductors to be dependent on the extrinsically controlled properties of doping level and defect concentration rather than the intrinsic particle shape and size[57,65] making them well suited as PTT agents. For example, tungsten bronze nanoparticle compounds with an LSPR in the NIR such as $Cs_xWO_3$ (Fig. 2) are shown[66] to be effective PPT agents, reaching 46°C in less than 15 minutes under a low irradiance (0.7 W/cm$^2$). Furthermore, many semiconducting nanoparticles used for PTT are known to be biocompatible and biodegradable[67–69]. Elemental silicon has been shown to be biocompatible in human subjects and will biodegrade into soluble silicic acid followed by urinary excretion with a half-life of less than 3 hours for 90% of the absorbed silicon[70]. For these reasons, many semiconducting nanoparticles have been examined as potential PTT agents, including copper chalcogenides[58,59,67,71–74], cadmium chalcogenides[75], transition-metal oxides[61,62,66,76–78], bismuth selenide[79,80], germanium[81], and silicon[64,68,82–84].

Of the semiconductors mentioned above, the copper chalcogenides have gained the most attention; specifically copper sulfide (CuS). These materials were originally studied as bio-compatible, nontoxic alternatives to cadmium chalcogenide contrast agents[58,71,85]. Additionally, these low-cost, easily synthesized nanoparticles have been shown to have highly tunable LSPRs from ~800-1400 nm by adjusting their stoichiometry to make the material more or less copper deficient[86,87]. The particles are also shown to have a high thermal stability and PT conversion efficiencies greater than Au nanoparticles (~22-60%)[58,67]. One downfall, however, is that copper chalcogenides are generally hydrophobic and require subsequent capping or coating chemistry to make them hydrophilic[59].

The primary difference between modelling photothermal heating for semiconducting nanomaterials relative to metallic counterparts is that semiconducting structures typically allow for substantial penetration of electromagnetic fields throughout the internal volume of the particle. Generally, the source term $Q(\mathbf{r},t)$ is dependent on the complex internal electric

fields generated by irradiation as well as the electrical conductivity at optical frequencies and is given by[88]:

$$Q(\mathbf{r},t) = \frac{1}{2}\sigma\tilde{\mathbf{E}}(\mathbf{r},\mathbf{t})\cdot\tilde{\mathbf{E}}^{*}(\mathbf{r},\mathbf{t}) \quad (4)$$

where $\mathbf{E}(\mathbf{r},t)$ and $\mathbf{E}^{*}(\mathbf{r},t)$ are the generated electric field within the NP and its complex conjugate, respectively[88]. The electrical conductivity at optical frequencies is given by[89]:

$$\sigma = \frac{4\pi nk}{\lambda_i \mu c} \quad (5)$$

where $\lambda_i$ is the incident wavelength, $\mu$ is the nanoparticles relative magnetic permeability, $c$ is the speed of light, and $n$ and $k$ are the real and imaginary parts of the index of refraction of the nanoparticle, respectively[88].

By analyzing equations (1), (4), and (5), one can see that the photothermal heating of a semiconducting nanostructure is affected by the intensity of the incident light, the particle's internal electromagnetic field distribution, and also by the material's thermal and electrical conductivity. For instance, the magnitude of internal electric fields can be increased for constant incident irradiance by tuning the nanoparticle size to a morphology-dependent resonance (MDR)[89–91]. Additionally, the effective photothermal heating efficiency of an irradiated nanoparticle has been shown to be highly dependent on its defect concentration which can be altered using methods such as ion implantation[64]. The defects act as recombination centers for generated bound excitons as well as scattering sites for both charge carriers and phonons. The defects thus alter both the electrical and thermal[92] conductivity of the nanoparticles.

An interesting class of materials that have recently been identified as potential PTT agents are 3D topological insulators[79,80]. Topological insulators have insulating bulk properties with nontrivial, conducting surface and boundary states. As one such material, bismuth selenide ($Bi_2Se_3$), has recently[79] been shown to be an effective absorber of NIR light and converts that light into heat efficiently, making it an effective PPT agent. Furthermore, the same nanoparticles showed strong X-ray attenuation characteristics, making it double as a multifunctional X-ray computed tomography imaging agent (Fig. 3).

These semiconducting nanoparticles have also been coupled with other materials to make multifunctional theranostic nanoparticles[93–95]. In a recent study, ultrasmall CuS nanoparticles were attached at the surface of a silica covered rare-earth upconverting nanoparticle ($NaF_4Yb_{0.78}Er_{0.02}Gd_{0.20}@SiO_2\text{-}NH_2$)[95]. The ultrasmall CuS nanoparticles work as efficient photothermal agents at the tumor cite. Furthermore, the generated heat from the CuS nanoparticles works synergistically with the high-Z radiotherapy enhancing elements Yb, Er, and Gd by potentially increasing intratumoral blood flow which has been shown to increase tumor cell sensitivity to radiotherapy[95].

In another study involving CuS, the nuclide $^{64}Cu$ was integrated during synthesis of CuS to create [$^{64}Cu$]CuS nanoparticles[74]. The radioactive $^{64}Cu$ was added during the synthesis of

the nanoparticles, resulting in the synthesis of multifunctional nanoparticles without the need to chelate on the radioisotope. In this case, the radioisotope $^{64}$Cu was shown to double as an efficient PET imaging agent after being embedded within its nanocrystalline semiconducting host particle[74].

## Carbon Materials

Nanoscale carbon materials[96] including carbon nanotubes[97], graphene[98] / graphene-oxide[99], and nanodiamond[100], and have also received a significant amount of attention in recent years for combining photothermal therapy with other multimodal diagnostic platforms. These materials frequently are categorized based on both their nanoscale morphologies and relative abuncance of $sp^2$- and $sp^3$- covalent bonds found in a given structure. Graphene and carbon nanotube based materials represent the limit of complete $sp^2$ bonding where each carbon atom is connected to three others in a flat, hexagonal, π-conjugated network.

Single-walled carbon nanotubes (SWCNTs) can be considered to be formed by rolling a two dimensional sheet of graphene into a tube with or without a 'twist' in the sheet of carbon atoms. Interestingly, SWCNTs may exhibit either semiconducting or metallic electronic structure based on the extent to which a sheet of graphene is twisted while being rolled to make a tube[101]. The one dimensional morphology of SWCNTs leads to sharp spikes in the density of electronic states (van Hove singularities) that create large absorption coefficients in the near-infrared[101]. SWCNTs efficiently convert absorbed electromagnetic energy (including at radio frequencies[102]) to release significant amounts of heat for applications in photothermal therapy[103] and photoacoustic[104] imaging (PAI). Similar to SWCNTs, single-walled carbon nanohorns (SWCNHs) were recently[105] shown to possess potential as a PTT and PAI agent. Chen et al. conjugated the SWCNHs with a branched polymer ($C_{18}$PMH-PEG) for improved biocompatibility and circulation. After intravenously injecting tumor bearing mice with functionalized SWCNHs and irradiating with an 808 nm laser for 10 min. at a power density of 0.4 W $cm^{-2}$ they observed intratumoral temperatures as high as 55°C and tumor ablation as opposed to irradiated mice with injections of $C_{18}$PMH-PEG only (Fig. 4).

Beyond photothermal heating, near-infrared excitation of semiconducting SWCNTs also generates bright NIR photoluminescence which can be used for diagnostic optical imaging[106,107]. SWCNTs have also been labeled with radioisotopes such as $^{111}$In that can be used for quantitative γ-ray counting of the concentration of residual nanomaterials within specific in vivo organ tissue. Near infrared excitation of SWCNTs also has been demonstrated to generate reactive oxygen species that acts as a complementary photodynamic approach for damaging tumor cells[108]. Targeting and selectivity during cancer cell destruction has also been reported through molecular surface functionalization of SWCNTs. For instance, adding a folate[109] moiety allows for selective internalization of SWCNTs inside cells labeled with a folate receptor tumor marker, reducing the effect of photothermal heating on healthy tissues. Surface functionalization has also been shown to increase the biocompatiblity of SWCNTs, both in vitro and in vivo[110].

In contrast to carbon nanotubes, nanodiamond[111] materials represent the limit of nearly complete $sp^3$ bonding where carbon atoms form a three-dimensional crystal based on a face-

centered cubic (FCC) Bravais lattice and a diatomic basis of tetrahedrally bonded carbon atoms with atomic coordinates of (0,0,0) and ($\frac{1}{4}, \frac{1}{4}, \frac{1}{4}$). Diamond nanocrystals can be produced with many different methods including the detonation of high explosives[100], high-pressure high-temperature processing[112,113], pulsed laser ablation, or more recently through direct-current atmospheric pressure plasmas[114] where grain sizes can range from single-digit nanometers to several hundred nanometers, depending on the synthetic method. The wide band gap of diamond (5.5 eV) means these materials can be considered transparent insulators at visible and near-infrared wavelengths, although ion irradiation has been demonstrated to create a large number of point defects and graphitization[115] in the diamond lattice, leading to enhanced optical absorption that could be used for photothermal therapy. More recently, novel composite nanostructures of diamond with coatings of gold and silver have been demonstrated to exhibit ehanced optical absorption for PTT[48].

Ion irradiation of nanodiamonds has also been shown to assist in the formation[116] of the well-known negatively-charged nitrogen-vacancy point defect center with a bright and photostable characteristic zero-phonon emission maximum of $\lambda$ =637 nm. It also has been shown that nanodiamond materials are highly biocompatible[117], and are readily endocytosed by numerous in vitro tissue models[118] and in vivo model organisms[119]. Several physiologically active small-molecules, including daunorubicin[120], epirubicin[118], polymyxin B[121], and bone forming proteins[122] also have been demonstrated to adsorb non-specifically on the surface of nanodiamonds for release in tissue[123].

## Iron Oxide Nanocrystals

Magnetic particle hyperthermia has been studied for more than 50 years with the first clinical trial demonstrating its effectiveness on prostate cancer and gliomas[124] in 1957. The past decade has seen a marked increase in clinical trial studies[125–128]. Much like the metallic and semiconducting nanoparticles, hyperthermal therapy via magnetic particles consists of localization, nanoparticle heating, and subsequent conduction of heat into the surrounding tissue, raising the local temperature above 42°C. The difference between the magnetic particles and their metallic and semiconducting counterparts is the mechanism by which the particle is heated. Briefly, magnetic hyperthermia is achieved by applying external alternating magnetic fields to cause the magnetic particles to heat through hysteresis loss (Néel relaxation) or induced eddy currents[129–132].

For multidomain particles, the largest contribution to heating is hysteresis loss[133] which itself can be described by two further mechanisms. The first is due to the rotation of magnetic moments inside a single domain while the second is from domain walls pinned on the impurities inside the materials. The process is irreversible and energy losses occur as the amplitude of the applied AC magnetic field is increased[133]. Under the influence of the time-varying magnetic field, the hysteretic properties of ferrimagnetic (FM) materials can be used to describe the heat generated per unit volume ($P_{FM}$)[134]:

$$P_{FM} = \mu_0 f \oint H dM \quad (6)$$

where $\mu_0$ is the permeability of free space, $f$ is the frequency of the applied magnetic field, $H$ is the magnetic field strength and $M$ is the magnetization, which is magnetic moment per unit volume.

For single domain particles, the rotation of magnetic moments is the main source of hyperthermal heating[135]. Below a certain particle size (superparamagnetic size, SPM), the multidomain particles become energetically unfavourable and each particle behaves as a single magnetic domain[136,137]. As the external magnetic field is applied, the magnetic moment reorients along the magnetic field axis. Once the magnetic field is removed, the magnetic moment relaxes to its equilibrium orientation dissipating energy and, thereby, generates heat. If the rotation in question is of the magnetic moment within the particle, the process is called Néel relaxation[138]. The relaxation time $\tau_N$ describes this process and was proposed by Louis Néel in 1949 with the relation to temperature, $T$:

$$\tau = \tau_0 e^{\frac{E_B}{k_B T}} \quad (7)$$

where $\tau_0$, is the attempt time, $k_B$ is Boltzmann constant and $E_B$ is the anisotropy energy barrier.

Similar to Néel relaxation, if the particle itself rotates relative to its surrounding medium under the influence of a magnetic field, it will undergo Brownian relaxation[139], which depends on both the particle and medium properties. The Brownian relaxation time is described[135] as:

$$\tau_B = \frac{3\tau_0 V_h \eta(T)}{k_B T} \quad (8)$$

where $V_h$ is the hydrodynamic volume and $\eta(T)$ is the viscosity of the medium.

The SPM size prevents agglomeration of particles in the absence of a coercive force or remanent field, which may increase the residence time of particles within a patient's body[134]. The heating power of magnetic hyperthermia can be controlled easily by both the AC magnetic field's amplitude and the concentration of nanoparticles at the tumor site[141–143]. Therefore, iron oxide SPM particles have been widely used in medical research owing to their non-toxicity, biocompatibility, and large magnetic response. Khandhar et al.[144] have optimized the size of the magnetic nanoparticles at a particular AC magnetic field frequency to enhance its magnetic hyperthermia potential. Sadhukha et al.[145] developed inhalable magnetic particles for targeting lung cancer cells, which successfully demonstrated prevention of the tumor growth. In 2014, Tsiapa et al. developed and evaluated iron oxide nanoparticles coated with aminosilane as a cancer hyperthermia therapy agent. Fig. 5 shows that the in vivo study with mice can reach ablative temperatures[140]

Recently, photothermal effects of magnetic, iron oxide-based nanoparticles have also attracted a great interest. Compared to the traditional magnetic hyperthermia, which requires a high voltage and current to focus a magnetic field in a large air volume, photothermal ablation needs only NIR light to trigger this process with deeper penetration and higher efficiency[27,28]. One study demonstrated the potential of magnetic iron-oxide particles for

PTT where surface-functionalized $Fe_3O_4$ particles were introduced to esophageal tumors in mice and irradiated with NIR light[146]. A histological assessment of the treated and untreated tissues is shown in Figure 6. Iron oxide particles have the added benefit of being used for multifunctional applications in diagnosis and real-time monitoring of deep tissues with magnetic resonance imaging (MRI)[29].

To increase the absorption of NIR light and enhance the particle's functionality, magnetic nanocrystals can be synthesized with various coatings and ligands, such as gold[147–149], silica[150], carbon nanotubes[151], polymers[94,146,152], $TiO_2$[153], Ag[148,154], graphitic carbon[29,94], and upconversion crystals[155–159]. The surface of magnetic particles can also be modified to be porous. Kim et al.[160] synthesized monodisperse mesoporous nanoparticles which consist of a single magnetite nanocrystal core and mesoporous silica shell. The porous, biocompatible shell can be loaded with drugs to assist in hyperthermal therapy. They can also be loaded with fluorescent dyes to help image the outcomes of cancer therapy. The absorption of NIR light can also be tuned by the surface modification. Liao et al.[150] designed a ligand-assisted synthesis of NIR activated magnetite nanoparticles, which have increased d-d transition probability of iron ions at NIR wavelengths. The absorption wavelength can also be tuned during the synthesis.

One of the most common composite materials for photothermal therapy is based on a gold/magnetite composite nanostructure. Larson et al.[147] used gold-coated iron oxide nanoparticles to enhance both MRI and optical imaging of breast cancer cells followed by effective photothermal ablation of the same cells. The surface plasmon resonance of the gold layer provides optical contrast through the scattering of visible light. The gold layer also has strong optical NIR absorption, which makes the nanoparticles promising agents for PTT. In addition, the iron oxide cores show strong T2 contrast (spin-spin relaxation time), which can be tested with clinical MRI.

Magnetic hyperthermia and NIR PTT of magnetic materials both have promising futures but further improvements are needed before either can be applied clinically. One of the main obstacles is the precise control of local hyperthermal temperatures. It is also crucial that the material is biocompatible and stable in tumor tissues while preventing collateral damage to surrounding, non-cancerous tissues[161].

## Conclusions

This review highlights a range of metallic, semiconducting, and insulating materials that have been reported in recent years that combine electromagnetic hyperthermal heating with a variety of diagnostic capabilities with an aim of treating a variety of aggressive strains of cancer. Nanoscale materials have been demonstrated to offer a variety of therapeutic and diagnosic (theranostic) capabilities based on combining traditional small-molecule pharmaceuticals with photothermal heating, radiation therapy, advanced optical- and radio-imaging, and also tumor targeting via molecular surface function-alziation. Although we have reviewed the operative heating mechanisms for several of the most widely studied nanomaterials, the number and variety of recent publications is too vast to make possible a comprehensive discussion in this mini-review. However, there are several recently-published

reviews that we would like to point the interested reader to given the space constraints here: $YLiF_4$[162], $NaYF_4$[163–168], silver nanocrystals[169–172], palladium nanocrystals[173–175], nanocrystalline metal alloys[176–179], and $SiO_2$[180,181].

The potential of nanoparticles in PTT is promising given the wide range of materials available. However, their use in clinical treatments will require further studies to better understand relative advantages and disadvantages, including: bio-compatibility, functionality, heat dissipation in various tissues, and interaction with light, especially within the NIR tissue transparency window. Gold is a substantial absorber, but the high cost of feedstocks may limit its widespread usage. Furthermore, the plasmon resonances in metals are affected by the size and shape of the particle and are susceptible to drift. Semiconductor absorption is more stable and can be controlled with doping, but the materials are often composed of toxic metals. Future research of semiconductors as PTT agents will certainly require the study of biocompatible materials. Carbon can be much cheaper and also has a significant absorption cross section (in $sp^2$ form), but the chirality and diameter of nanotubes, which severely impact the physical and chemical properties, are difficult to control. Magnetic hyperthermia often uses materials that are biocompatible; however, particle size polydispersity reduces heating efficiency. Additionally, the alternating magnetic fields required to heat the particles can have negative effects on healthy tissue. It is clear that there is no perfect material fo PTT, but researchers everywhere continue to search for the best methods for synthesizing high-yield, monodisperse hypthermal therapy agents. Given the global extent of interest in this field, the base of fundamental scientific knowledge regarding the physical- and toxicological- properties of hyperthermal nanomaterials continues to grow more each day. Several novel ideas for combining hyperthermal heating with multifunctional in vivo diagnostics discussed in this mini-review have great potential to impact the clinical treatment of solid tumors in the future.

## Acknowledgements

This research was made possible by a grant from the Air Force Office of Scientific Research Young Investigator Program (contract #FA95501210400) and start-up funding from the University of Washington. B.E.S. acknowledges support from an NIH T32 training fellowship. P.B.R. thanks the NSF for a Graduate Research Fellowship under grant number DGE-1256082. P.J.P. gratefully acknowledges support from the Pacific Northwest National Laboratory which is operated by the Battelle Memorial Institute for the US DOE under contract DE-AC 06-76RLO 1830.

## References

1. Kim BY, Rutka JT, Chan WC. New England Journal of Medicine. 2010; 363:2434–2443. [PubMed: 21158659]
2. Breasted, JH. The Edwin Smith Surgical Papyrus: Hieroglyphic transliterations, translation and commentary. University of Chicago Press; 1930.
3. Sato M, Watanabe Y, Ueda S, Iseki S, Abe Y, Sato N, Kimura S, Okubo K, Onji M. Gastroenterology. 1996; 110:1507–1514. [PubMed: 8613057]
4. Mirza A, Fornage B, Sneige N, Kuerer H, Newman L, Ames F, Singletary E. Cancer Journal. 2001; 7:95–95.
5. Wu F, Chen W-Z, Bai J, Zou J-Z, Wang Z-L, Zhu H, Wang Z-B. Ultrasound in Medicine and Biology. 2001; 27:1099–1106. [PubMed: 11527596]
6. Maiman TH. Nature. 1960; 187:493–494.
7. Anderson RR, Parrish JA. Science. 1983; 220:524–527. [PubMed: 6836297]

8. Landsman ML, Kwant G, Mook GA, Zijlstra WG. Journal of Applied Physiology. 1976; 40:575–583. [PubMed: 776922]
9. Chen WR, Adams RL, Heaton S, Dickey DT, Bartels KE, Nordquist RE. Cancer Letters. 1995; 88:15–19. [PubMed: 7850768]
10. Jaque D, Maestro LM, Rosal B. d. Haro-Gonzalez P, Benayas A, Plaza JL, Rodríguez EM, Solé JG. Nanoscale. 2014; 6:9494–9530. [PubMed: 25030381]
11. Govorov AO, Zhang W, Skeini T, Richardson H, Lee J, Kotov NA. Nanoscale Research Letters. 2006; 1:84.
12. Boca SC, Potara M, Gabudean A-M, Juhem A, Baldeck PL, Astilean S. Cancer Letters. 2011; 311:131–140. [PubMed: 21840122]
13. C S R, Kumar J, R. V, V. M, Abraham A. Pharmacological research: the official journal of the Italian Pharmacological Society. 2012; 65:261–269.
14. Huang X, El-Sayed MA. Journal of Advanced Research. 2010; 1:13–28.
15. Govorov AO, Richardson HH. Nano Today. 2007; 2:30–38.
16. Zhang Z, Wang J, Chen C. Theranostics. 2013; 3:223–238. [PubMed: 23471510]
17. Gannon CJ, Patra CR, Bhattacharya R, Mukherjee P, Curley SA. Journal of Nanobiotechnology. 2008; 6:2. [PubMed: 18234109]
18. Collins CB, McCoy RS, Ackerson BJ, Collins GJ, Ackerson CJ. Nanoscale. 2014; 6:8459–8472. [PubMed: 24962620]
19. Link S, El-Sayed MA. The Journal of Physical Chemistry B. 1999; 103:8410–8426.
20. Gao L, Liu R, Gao F, Wang Y, Jiang X, Gao X. ACS Nano. 2014:7260–7271. [PubMed: 24992260]
21. Wu X, Wang J, Chen J-Y. Plasmonics. 2013; 8:685–691.
22. Lim D-K, Barhoumi A, Wylie RG, Reznor G, Langer RS, Kohane DS. Nano Letters. 2013; 13:4075–4079. [PubMed: 23899267]
23. Link S, El-Sayed MA. The Journal of Physical Chemistry B. 1999; 103:4212–4217.
24. Shen J, Kim H-C, Mu C, Gentile E, Mai J, Wolfram J, Ji L.-n. Ferrari M, Mao Z.-w. Shen H. Advanced Healthcare Materials. 2014; 3:1629–1637. [PubMed: 24692076]
25. Baldwin CL, Bigelow NW, Masiello DJ. The Journal of Physical Chemistry Letters. 2014; 5:1347–1354. [PubMed: 26269978]
26. Dickerson EB, Dreaden EC, Huang X, El-Sayed IH, Chu H, Pushpanketh S, McDonald JF, El-Sayed MA. Cancer letters. 2008; 269:57–66. [PubMed: 18541363]
27. Cho EC, Glaus C, Chen J, Welch MJ, Xia Y. Trends in Molecular Medicine. 2010; 16:561–573. [PubMed: 21074494]
28. Mahmoudi M, Serpooshan V, Laurent S. Nanoscale. 2011; 3:3007. [PubMed: 21717012]
29. Seo WS, Lee JH, Sun X, Suzuki Y, Mann D, Liu Z, Terashima M, Yang PC, McConnell MV, Nishimura DG, Dai H. Nature Materials. 2006; 5:971–976. [PubMed: 17115025]
30. Jana NR, Gearheart L, Murphy CJ. Advanced Materials. 2001; 13:1389–1393.
31. Zhao T, Yu K, Li L, Zhang T, Guan Z, Gao N, Yuan P, Li S, Yao SQ, Xu Q-H, Xu GQ. ACS Applied Materials & Interfaces. 2014; 6:2700–2708. [PubMed: 24483257]
32. Chuang Y-C, Lin C-J, Lo S-F, Wang J-L, Tzou S-C, Yuan S-S, Wang Y-M. Biomaterials. 2014; 35:4678–4687. [PubMed: 24613648]
33. Zhao Y, Sultan D, Detering L, Cho S, Sun G, Pierce R, Wooley KL, Liu Y. Angewandte Chemie (International Ed. in English). 2014; 53:156–159. [PubMed: 24272951]
34. Wang J-H, Wang B, Liu Q, Li Q, Huang H, Song L, Sun T-Y, Wang H, Yu X-F, Li C, Chu PK. Biomaterials. 2013; 34:4274–4283. [PubMed: 23489924]
35. Nima ZA, Mahmood M, Xu Y, Mustafa T, Watanabe F, Nedosekin DA, Juratli MA, Fahmi T, Galanzha EI, Nolan JP, Basnakian AG, Zharov VP, Biris AS. Scientific Reports. 2014:4.
36. Wu X, Chen J-Y, Brech A, Fang C, Wang J, Helm PJ, Peng Q. Biomaterials. 2013; 34:6157–6162. [PubMed: 23706782]
37. Gormley AJ, Larson N, Banisadr A, Robinson R, Frazier N, Ray A, Ghandehari H. Journal of Controlled Release. 2013; 166:130–138. [PubMed: 23262203]

38. Dembereldorj U, Choi SY, Ganbold E-O, Song NW, Kim D, Choo J, Lee SY, Kim S, Joo S-W. Photochemistry and Photobiology. 2014; 90:659–666. [PubMed: 24303894]
39. Buckway B, Frazier N, Gormley AJ, Ray A, Ghandehari H. Nuclear Medicine and Biology. 2014; 41:282–289. [PubMed: 24461626]
40. Liopo AV, Conjusteau A, Konopleva M, Andreeff M, Oraevsky AA. Nano biomedicine and engineering. 2012; 4:66–75. [PubMed: 22720194]
41. Vivero-Escoto JL, Slowing II, Wu C-W, Lin VS-Y. Journal of the American Chemical Society. 2009; 131:3462–3463. [PubMed: 19275256]
42. Kyrsting A, Bendix PM, Stamou DG, Oddershede LB. Nano Letters. 2011; 11:888–892. [PubMed: 21188965]
43. Ghosh P, Han G, De M, Kim CK, Rotello VM. Advanced Drug Delivery Reviews. 2008; 60:1307–1315. [PubMed: 18555555]
44. Cheng Y, Samia AC, Meyers JD, Panagopoulos I, Fei B, Burda C. Journal of the American Chemical Society. 2008; 130:10643–10647. [PubMed: 18642918]
45. Alkilany AM, Thompson LB, Boulos SP, Sisco PN, Murphy CJ. Advanced Drug Delivery Reviews. 2012; 64:190–199. [PubMed: 21397647]
46. Dreaden EC, Mwakwari SC, Austin LA, Kieffer MJ, Oyelere AK, El-Sayed MA. Small. 2012; 8:2819–2822. [PubMed: 22777707]
47. Norman RS, Stone JW, Gole A, Murphy CJ, Sabo-Attwood TL. Nano Letters. 2008; 8:302–306. [PubMed: 18062714]
48. Cheng L-C, Chen HM, Lai T-C, Chan Y-C, Liu R-S, Sung JC, Hsiao M, Chen C-H, Her L-J, Tsai DP. Nanoscale. 2013; 5:3931–3940. [PubMed: 23536050]
49. Skala MC, Squirrell JM, Vrotsos KM, Eickhoff JC, Gendron-Fitzpatrick A, Eliceiri KW, Ramanujam N. Cancer Research. 2005; 65:1180–1186. [PubMed: 15735001]
50. Resch-Genger U, Grabolle M, Cavaliere-Jaricot S, Nitschke R, Nann T. Nature Methods. 2008; 5:763–775. [PubMed: 18756197]
51. Huang X, El-Sayed IH, Qian W, El-Sayed MA. Journal of the American Chemical Society. 2006; 128:2115–2120. [PubMed: 16464114]
52. Durr NJ, Larson T, Smith DK, Korgel BA, Sokolov K, Ben-Yakar A. Nano Letters. 2007; 7:941–945. [PubMed: 17335272]
53. Angelatos AS, Radt B, Caruso F. The Journal of Physical Chemistry B. 2005; 109:3071–3076. [PubMed: 16851322]
54. Jain RK, Stylianopoulos T. Nature Reviews Clinical Oncology. 2010; 7:653–664.
55. Pasparakis G. Small. 2013; 9:4130–4134. [PubMed: 23813944]
56. Vankayala R, Sagadevan A, Vijayaraghavan P, Kuo C-L, Hwang KC. Angewandte Chemie International Edition. 2011; 50:10640–10644.
57. Faucheaux JA, Stanton ALD, Jain PK. The Journal of Physical Chemistry Letters. 2014; 5:976–985. [PubMed: 26270976]
58. Hessel CM, Pattani VP, Rasch M, Panthani MG, Koo B, Tunnell JW, Korgel BA. Nano letters. 2011; 11:2560–2566. [PubMed: 21553924]
59. Li W, Zamani R, Rivera Gil P, Pelaz B, Ibez M, Cadavid D, Shavel A, Alvarez-Puebla RA, Parak WJ, Arbiol J, Cabot A. Journal of the American Chemical Society. 2013; 135:7098–7101. [PubMed: 23647089]
60. Zhao Y, Burda C. Energy & Environmental Science. 2012; 5:5564–5576.
61. Chen Z, Wang Q, Wang H, Zhang L, Song G, Song L, Hu J, Wang H, Liu J, Zhu M, Zhao D. Advanced Materials. 2013; 25:2095–2100. [PubMed: 23427112]
62. Song G, Shen J, Jiang F, Hu R, Li W, An L, Zou R, Chen Z, Qin Z, Hu J. ACS Applied Materials & Interfaces. 2014; 6:3915–3922. [PubMed: 24564332]
63. Chou L-W, Shin N, Sivaram SV, Filler MA. Journal of the American Chemical Society. 2012; 134:16155–16158. [PubMed: 22985223]
64. Roder PB, Smith BE, Davis EJ, Pauzauskie PJ. The Journal of Physical Chemistry C. 2014; 118:1407–1416.

65. Young JK, Figueroa ER, Drezek RA. Annals of biomedical engineering. 2012; 40:438–459. [PubMed: 22134466]
66. Guo C, Yin S, Yu H, Liu S, Dong Q, Goto T, Zhang Z, Li Y, Sato T. Nanoscale. 2013; 5:6469–6478. [PubMed: 23743996]
67. Li B, Wang Q, Zou R, Liu X, Xu K, Li W, Hu J. Nanoscale. 2014; 6:3274–3282. [PubMed: 24509646]
68. Wang N, Yao BD, Chan YF, Zhang XY. Nano Letters. 2003; 3:475–477.
69. Park J-H, Gu L, von Maltzahn G, Ruoslahti E, Bhatia SN, Sailor MJ. Nature Materials. 2009; 8:331–336. [PubMed: 19234444]
70. Popplewell JF, King SJ, Day JP, Ackrill P, Fifield LK, Cresswell RG, di Tada ML, Liu K. Journal of Inorganic Biochemistry. 1998; 69:177–180. [PubMed: 9629677]
71. Li Y, Lu W, Huang Q, Li C, Chen W. Nanomedicine. 2010; 5:1161–1171. [PubMed: 21039194]
72. Song G, Wang Q, Wang Y, Lv G, Li C, Zou R, Chen Z, Qin Z, Huo K, Hu R, Hu J. Advanced Functional Materials. 2013; 23:4281–4292.
73. Tian Q, Hu J, Zhu Y, Zou R, Chen Z, Yang S, Li R, Su Q, Han Y, Liu X. Journal of the American Chemical Society. 2013; 135:8571–8577. [PubMed: 23687972]
74. Zhou M, Zhang R, Huang M, Lu W, Song S, Melancon MP, Tian M, Liang D, Li C. Journal of the American Chemical Society. 2010; 132:15351–15358. [PubMed: 20942456]
75. Chu M, Pan X, Zhang D, Wu Q, Peng J, Hai W. Biomaterials. 2012; 33:7071–7083. [PubMed: 22818982]
76. Lee C, Hong C, Kim H, Kang J, Zheng HM. Photochemistry and Photobiology. 2010; 86:981–989. [PubMed: 20408983]
77. Li B, Zhang Y, Zou R, Wang Q, Zhang B, An L, Yin F, Hua Y, Hu J. Dalton Transactions. 2014; 43:6244–6250. [PubMed: 24598863]
78. Zhou Z, Kong B, Yu C, Shi X, Wang M, Liu W, Sun Y, Zhang Y, Yang H, Yang S. Scientific Reports. 2014:4.
79. Li J, Jiang F, Yang B, Song X-R, Liu Y, Yang H-H, Cao D-R, Shi W-R, Chen G-N. Scientific Reports. 2013:3.
80. Yu Y, Sun W-T, Hu Z-D, Chen Q, Peng L-M. Materials Chemistry and Physics. 2010; 124:865–869.
81. Lambert T, Andrews N, Gerung H, Boyle T, Oliver J, Wilson B, Han S. Small. 2007; 3:691–699. [PubMed: 17299826]
82. Jiménez-Pérez JL, Sánchez-Ramírez JF, Cornejo-Monroy D, Gutierrez-Fuentes R, Rojas JAP, Cruz-Orea A, Algatti MA, Jacinto C. International Journal of Thermophysics. 2012; 33:69–79.
83. Lee C, Kim H, Hong C, Kim M, Hong SS, Lee DH, Lee WI. Journal of Materials Chemistry. 2008; 18:4790–4795.
84. Regli S, Kelly JA, Shukaliak AM, Veinot JGC. The Journal of Physical Chemistry Letters. 2012; 3:1793–1797. [PubMed: 26291861]
85. Derfus AM, Chan WCW, Bhatia SN. Nano Letters. 2004; 4:11–18.
86. Hsu S-W, Ngo C, Tao AR. Nano Letters. 2014; 14:2372–2380. [PubMed: 24738726]
87. Bryks W, Wette M, Velez N, Hsu S-W, Tao AR. Journal of the American Chemical Society. 2014; 136:6175–6178. [PubMed: 24712869]
88. Allen TM, Buehler MF, Davis EJ. Journal of Colloid and Interface Science. 1991; 142:343–356.
89. Roder PB, Pauzauskie PJ, Davis EJ. Langmuir. 2012; 28:16177–16185. [PubMed: 23061375]
90. Foss WR, Davis EJ. Chemical Engineering Communications. 1996; 152-153:113–138.
91. Popp J, Lankers M, Schaschek K, Kiefer W, Hodges JT. Applied Optics. 1995; 34:2380. [PubMed: 21037793]
92. Wang T, Madsen GKH, Hartmaier A. Modelling and Simulation in Materials Science and Engineering. 2014; 22:035011.
93. Hu K-W, Jhang F-Y, Su C-H, Yeh C-S. Journal of Materials Chemistry. 2009; 19:2147–2153.
94. Huang C-C, Su C-H, Li W-M, Liu T-Y, Chen J-H, Yeh C-S. Advanced Functional Materials. 2009; 19:249–258.

95. Xiao Q, Zheng X, Bu W, Ge W, Zhang S, Chen F, Xing H, Ren Q, Fan W, Zhao K, Hua Y, Shi J. Journal of the American Chemical Society. 2013; 135:13041–13048. [PubMed: 23924214]
96. Liu Z, Robinson JT, Tabakman SM, Yang K, Dai H. Materials Today. 2011; 14:316–323.
97. Antaris AL, Robinson JT, Yaghi OK, Hong G, Diao S, Luong R, Dai H. ACS Nano. 2013; 7:3644–3652. [PubMed: 23521224]
98. Yang K, Feng L, Hong H, Cai W, Liu Z. Nature Protocols. 2013; 8:2392–2403. [PubMed: 24202553]
99. Wu M-C, Deokar AR, Liao J-H, Shih P-Y, Ling Y-C. ACS Nano. 2013; 7:1281–1290. [PubMed: 23363079]
100. Mochalin VN, Shenderova O, Ho D, Gogotsi Y. Nature Nanotechnology. 2012; 7:11–23.
101. Saito, R.; Dresselhaus, MS., editors. Physical Properties of Carbon Nanotubes. Imperial College Press; London: 1998.
102. Gannon CJ, Cherukuri P, Yakobson BI, Cognet L, Kanzius JS, Kittrell C, Weisman RB, Pasquali M, Schmidt HK, Smalley RE, Curley SA. Cancer. 2007; 110:2654–2665. [PubMed: 17960610]
103. Hashida Y, Tanaka H, Zhou S, Kawakami S, Yamashita F, Murakami T, Umeyama T, Imahori H, Hashida M. Journal of Controlled Release. 2014; 173:59–66. [PubMed: 24211651]
104. Kim J-W, Galanzha EI, Shashkov EV, Moon H-M, Zharov VP. Nature nanotechnology. 2009; 4:688–94.
105. Chen D, Wang C, Nie X, Li S, Li R, Guan M, Liu Z, Chen C, Wang C, Shu C, Wan L. Advanced Functional Materials. 2014; 24:6621–6628.
106. Welsher K, Liu Z, Daranciang D, Dai H. Nano Letters. 2008; 8:586–590. [PubMed: 18197719]
107. Robinson JT, Welsher K, Tabakman SM, Sherlock SP, Wang H, Luong R, Dai H. Nano Research. 2010; 3:779–793. [PubMed: 21804931]
108. Murakami T, Nakatsuji H, Inada M, Matoba Y, Umeyama T, Tsujimoto M, Isoda S, Hashida M, Imahori H. Journal of the American Chemical Society. 2012; 134:17862–17865. [PubMed: 23083004]
109. Huang H, Yuan Q, Shah JS, Misra RDK. Advanced Drug Delivery Reviews. 2011; 63:1332–1339. [PubMed: 21514336]
110. Schipper ML, Nakayama-Ratchford N, Davis CR, Kam NWS, Chu P, Liu Z, Sun X, Dai H, Gambhir SS. Nature Nanotechnology. 2008; 3:216–221.
111. Osawa E. Handb. Adv. Ceram. (2nd Ed.). 2013:89–102.
112. Pauzauskie PJ, Crowhurst JC, Worsley MA, Laurence TA, Kilcoyne ALD, Wang Y, Willey TM, Visbeck KS, Fakra SC, Evans WJ, Zaug JM, Satcher JH. Proceedings of the National Academy of Sciences. 2011; 108:8550–8553.
113. Mandal M, Haso F, Liu T, Fei Y, Landskron K. Chemical Communications. 2014; 50:11307–11310. [PubMed: 25116196]
114. Kumar A, Ann Lin P, Xue A, Hao B, Khin Yap Y, Sankaran RM. Nature Communications. 2013; 4:2618.
115. Klokov A, Tsvetkov V, Sharkov A, Aminev D, Khmelnitskiy R. Journal of Physics: Conference Series. 2014; 520:012006.
116. Fu C-C, Lee H-Y, Chen K, Lim T-S, Wu H-Y, Lin P-K, Wei P-K, Tsao P-H, Chang H-C, Fann W. Proceedings of the National Academy of Sciences. 2007; 104:727–732.
117. Schrand AM, Hens SAC, Shenderova OA. Critical Reviews in Solid State and Materials Sciences. 2009; 34:18–74.
118. Wang X, Low XC, Hou W, Abdullah LN, Toh TB, Mohd Abdul Rashid M, Ho D, Chow EK-H. ACS Nano. 2014; 8:12151–12166. [PubMed: 25437772]
119. Lin Y-C, Perevedentseva E, Tsai L-W, Wu K-T, Cheng C-L. Journal of Biophotonics. 2012; 5:838–847. [PubMed: 22815227]
120. Man HB, Kim H, Kim H-J, Robinson E, Liu WK, Chow EK-H, Ho D. Nanomedicine (New York, NY, United States). 2014; 10:359–369.
121. Mochalin VN, Pentecost A, Li X-M, Neitzel I, Nelson M, Wei C, He T, Guo F, Gogotsi Y. Molecular Pharmaceutics. 2013; 10:3728–3735. [PubMed: 23941665]

122. Moore L, Gatica M, Kim H, Osawa E, Ho D. Journal of Dental Research. 2013; 92:976–981. 6. [PubMed: 24045646]
123. Huang H, Pierstorff E, Osawa E, Ho D. Nano Letters. 2007; 7:3305–3314. [PubMed: 17918903]
124. Gilchrist RK, Medal R, Shorey WD, Hanselman R, Parrott J, Taylor CB. Annals of Surgery. 1957; 146:596–606. [PubMed: 13470751]
125. Johannsen M, Gneveckow U, Taymoorian K, Thiesen B, Waldfner N, Scholz R, Jung K, Jordan A, Wust P, Loening SA. International Journal of Hyperthermia. 2007; 23:315–323. [PubMed: 17523023]
126. Johannsen M, Gneveckow U, Thiesen B, Taymoorian K, Cho CH, Waldfner N, Scholz R, Jordan A, Loening SA, Wust P. European Urology. 2007; 52:1653–1662. [PubMed: 17125906]
127. Johannsen M, Thiesen B, Wust P, Jordan A. International Journal of Hyperthermia. 2010; 26:790–795. [PubMed: 20653418]
128. Maier-Hauff K, Ulrich F, Nestler D, Niehoff H, Wust P, Thiesen B, Orawa H, Budach V, Jordan A. Journal of Neuro-Oncology. 2011; 103:317–324. [PubMed: 20845061]
129. Hergt R, Andra W, d'Ambly C, Hilger I, Kaiser W, Richter U, Schmidt H-G. IEEE Transactions on Magnetics. 1998; 34:3745–3754.
130. Ugelstad, J.; Prestvik, WS.; Stenstad, P.; Kilaas, L.; Kvalheim, G. Selective cell separation with monosized magnetizable polymer beads Magnetism in Medicine ed H Nowak. Wiley-VCH; Berlin: 1998.
131. Wust P, Hildebrandt B, Sreenivasa G, Rau B, Gellermann J, Riess H, Felix R, Schlag P. The Lancet Oncology. 2002; 3:487–497. [PubMed: 12147435]
132. Gupta AK, Naregalkar RR, Vaidya VD, Gupta M. Nanomedicine. 2007; 2:23–39. [PubMed: 17716188]
133. Kronmüller, H.; Fähnle, M. Micromagnetism and the Microstructure of Ferromagnetic Solids. Cambridge University Press; 2003.
134. Pankhurst QA, Connolly J, Jones SK, Dobson J. Journal of Physics D: Applied Physics. 2003; 36:R167.
135. Ortega D, Pankhurst QA. Magnetic hyperthermia, The Royal Society of Chemistry. 2012
136. Thiesen B, Jordan A. International Journal of Hyperthermia. 2008; 24:467–474. [PubMed: 18608593]
137. Rivas J, Bañobre López M, Piẽiro Redondo Y, Rivas B, López-Quintela MA. Journal of Magnetism and Magnetic Materials. 2012; 324:3499–3502.
138. Néel L. Ann. Geophys. 1949; 5:99–136.
139. Brown WF Jr. Journal of Applied Physics. 1963; 34:1319–1320.
140. Tsiapa I, Efthimiadou EK, Fragogeorgi E, Loudos G, Varvarigou AD, Bouziotis P, Kordas GC, Mihailidis D, Nikiforidis GC, Xanthopoulos S, Psimadas D, Paravatou-Petsotas M, Palamaris L, Hazle JD, Kagadis GC. Journal of Colloid and Interface Science. 2014; 433:163–175. [PubMed: 25128864]
141. Brezovich IA. Medical Physics Monograph. 1988; 16:82–111.
142. Jordan A, Scholz R, Wust P, Fähling H, Krause J, Wlodarczyk W, Sander B, Vogl T, Felix R. International Journal of Hyperthermia. 1997; 13:587–605. [PubMed: 9421741]
143. Hilger I, Andr W, Hergt R, Hiergeist R, Schubert H, Kaiser WA. Radiology. 2001; 218:570–575. [PubMed: 11161180]
144. Khandhar AP, Ferguson RM, Simon JA, Krishnan KM. Journal of Biomedical Materials Research Part A. 2012; 100A:728–737. [PubMed: 22213652]
145. Sadhukha T, Wiedmann TS, Panyam J. Biomaterials. 2013; 34:5163–5171. [PubMed: 23591395]
146. Chu M, Shao Y, Peng J, Dai X, Li H, Wu Q, Shi D. Biomaterials. 2013; 34:4078–4088. [PubMed: 23465836]
147. Larson TA, Bankson J, Aaron J, Sokolov K. Nanotechnology. 2007; 18:325101.
148. Mandal M, Kundu S, Ghosh SK, Panigrahi S, Sau TK, Yusuf SM, Pal T. Journal of Colloid and Interface Science. 2005; 286:187–194. [PubMed: 15848416]

149. Urries I, Muñoz C, Gomez L, Marquina C, Sebastian V, Arruebo M, Santamaria J. Nanoscale. 2014; 6:9230–9240. [PubMed: 24980122]
150. Liao M-Y, Lai P-S, Yu H-P, Lin H-P, Huang C-C. Chemical Communications. 2012; 48:5319–5321. [PubMed: 22523747]
151. Wu H, Liu G, Wang X, Zhang J, Chen Y, Shi J, Yang H, Hu H, Yang S. Acta Biomaterialia. 2011; 7:3496–3504. [PubMed: 21664499]
152. Fang C, Kievit FM, Veiseh O, Stephen ZR, Wang T, Lee D, Ellenbogen RG, Zhang M. Journal of Controlled Release. 2012; 162:233–241. [PubMed: 22735239]
153. Islam MS, Kusumoto Y, Abdulla-Al-Mamun M, Horie Y. Catalysis Communications. 2011; 16:39–44.
154. Melnikov OV, Gorbenko OY, Markelova MN, Kaul AR, Atsarkin VA, Demidov VV, Soto C, Roy EJ, Odintsov BM. Journal of Biomedical Materials Research. Part A. 2009; 91:1048–1055. [PubMed: 19127514]
155. Jańczewski D, Zhang Y, Das GK, Yi DK, Padmanabhan P, Bhakoo KK, Tan TTY, Selvan ST. Microscopy Research and Technique. 2011; 74:563–576. [PubMed: 20734412]
156. Li Z, Zhang Y, Shuter B, Muhammad Idris N. Langmuir. 2009; 25:12015–12018. [PubMed: 19764797]
157. Kumar R, Nyk M, Ohulchanskyy TY, Flask CA, Prasad PN. Advanced Functional Materials. 2009; 19:853–859.
158. Zhou J, Sun Y, Du X, Xiong L, Hu H, Li F. Biomaterials. 2010; 31:3287–3295. [PubMed: 20132982]
159. Zhu X, Zhou J, Chen M, Shi M, Feng W, Li F. Biomaterials. 2012; 33:4618–4627. [PubMed: 22444645]
160. Kim J, Kim HS, Lee N, Kim T, Kim H, Yu T, Song IC, Moon WK, Hyeon T. Angewandte Chemie International Edition. 2008; 47:8438–8441.
161. Dutz S, Hergt R. International Journal of Hyperthermia. 2013; 29:790–800. [PubMed: 23968194]
162. Seletskiy DV, Melgaard SD, Bigotta S, Di Lieto A, Tonelli M, Sheik-Bahae M. Nature Photonics. 2010; 4:161–164.
163. Chatterjee DK, Fong LS, Zhang Y. Advanced Drug Delivery Reviews. 2008; 60:1627–1637. [PubMed: 18930086]
164. Chen H, Zhen Z, Todd T, Chu PK, Xie J. Materials Science & Engineering R-Reports. 2013; 74:35–69.
165. Cheng L, Wang C, Liu Z. Nanoscale. 2013; 5:23–37. [PubMed: 23135546]
166. Lin M, Zhao Y, Wang S, Liu M, Duan Z, Chen Y, Li F, Xu F, Lu T. Biotechnology Advances. 2012; 30:1551–1561. [PubMed: 22561011]
167. Wang F, Banerjee D, Liu Y, Chen X, Liu X. Analyst. 2010; 135:1839–1854. [PubMed: 20485777]
168. Wang F, Liu X. Chemical Society Reviews. 2009; 38:976–989. [PubMed: 19421576]
169. Austin LA, Mackey MA, Dreaden EC, El-Sayed MA. Archives of Toxicology. 2014; 88:1391–1417. [PubMed: 24894431]
170. Dement'eva O, Rudoy V. Colloid Journal. 2011; 73:724–742.
171. Menon JU, Jadeja P, Tambe P, Vu K, Yuan B, Nguyen KT. Theranostics. 2013; 3:152–166. [PubMed: 23471164]
172. Byeon JH, Kim Y-W. ACS Macro Letters. 2014; 3:205–210.
173. Huang X, Tang S, Mu X, Dai Y, Chen G, Zhou Z, Ruan F, Yang Z, Zheng N. Nature Nanotechnology. 2011; 6:28–32.
174. Xiao J-W, Fan S-X, Wang F, Sun L-D, Zheng X-Y, Yan C-H. Nanoscale. 2014; 6:4345–4351. [PubMed: 24622916]
175. Nie L, Chen M, Sun X, Rong P, Zheng N, Chen X. Nanoscale. 2014; 6:1271–1276. [PubMed: 24317132]
176. Boote BW, Byun H, Kim J-H. Journal of Nanoscience and Nanotechnology. 2014; 14:1563–1577. [PubMed: 24749442]

177. Huang X, Jain PK, El-Sayed IH, El-Sayed MA. Lasers in Medical Science. 2008; 23:217–228. [PubMed: 17674122]
178. Jain PK, Huang X, El-Sayed IH, El-Sayed MA. Plasmonics. 2007; 2:107–118.
179. Khlebtsov NG, Dykman LA. Journal of Quantitative Spectroscopy & Radiative Transfer. 2010; 111:1–35.
180. Piao Y, Burns A, Kim J, Wiesner U, Hyeon T. Advanced Functional Materials. 2008; 18:3745–3758.
181. Rosenholm JM, Sahlgren C, Lindén M. Nanoscale. 2010; 2:1870–1883. [PubMed: 20730166]

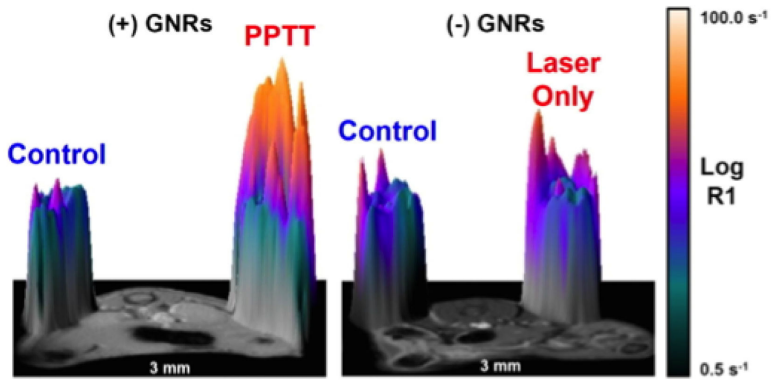


**Fig. 1.**

3D surface plot of magnetic resonance imaging (MRI) T1 relaxation scans. The left panel demonstrates the significant signal enhancement from a prostate tumor treated with AuNR NIR PTT resulting in an increase of gadolinium-labeled N-(2-hydroxypropyl)methylacrylimide accumulation relative to an untreated tumour within the same animal. The right panel shows that a tumour treated with a NIR laser alone has very little difference from the control tumour. Reprinted with permission from[37], Copyright 2013 Elsevier.

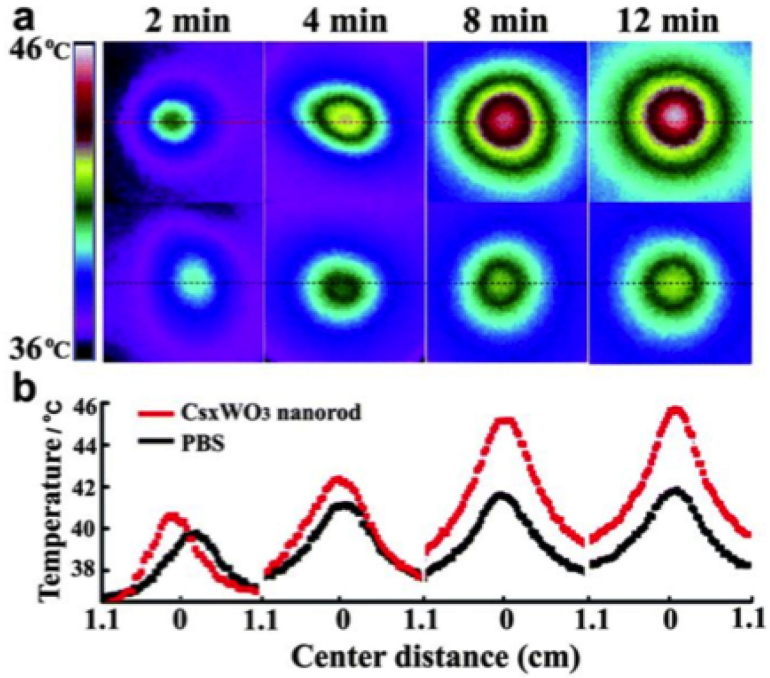


**Fig. 2.**

a) Time evolution of temperature distribution in A549 cells with $Cs_xWO_3$ nanorod-enrichment (top, 0.5 mg/mL) and without nanorod-enrichment (bottom). Cell dishes were irradiated at a wavelength of 980 nm at 200 mW (0.7 W/cm$^2$). Temperatures were measured with a thermographic meter. b) Cross sectional profiles of temperatures corresponding to the temperatures in (a). Reproduced with permission from[66], Copyright 2013 The Royal Society of Chemistry.

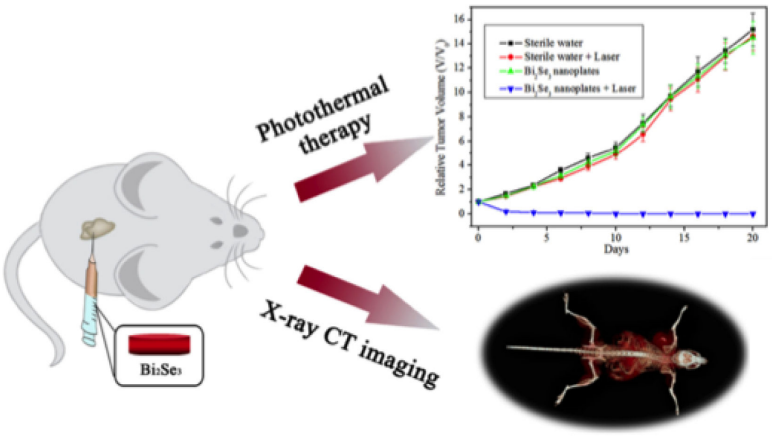


**Fig. 3.**

Topological insulating nanoparticles of $Bi_2Se_3$ are shown to be multifunctional in that they have shown to suppress growth (top graph) while also acting as an x-ray attenuator for computed tomography imaging (bottom image). Adapted from[79].

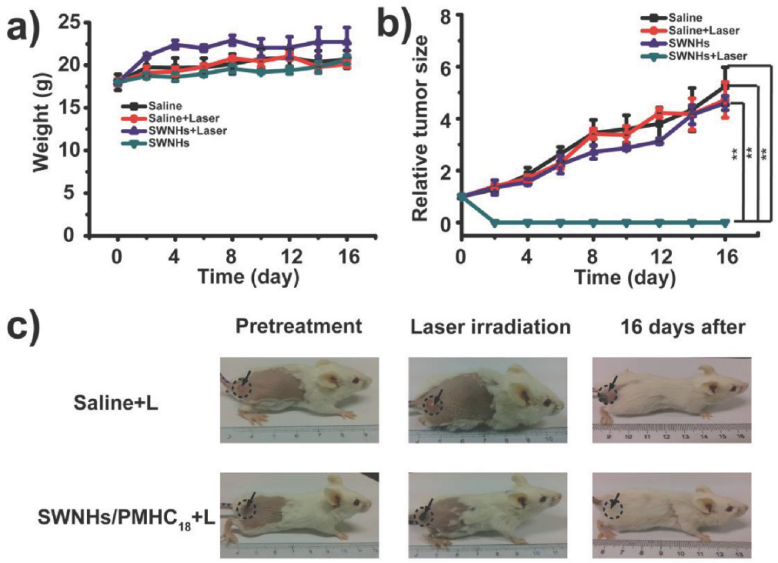


**Fig. 4.**

(a) Change in mice body weight after treatment. (b) Tumor growth curve after treatment. (c) Photographs of tumor bearing mice injected intravenously with either saline or SWCNHs/$C_{18}$PMH-PEG and exposed to laser treatment. Reproduced with permission from[105], Copyright 2014 Wiley-VCH.

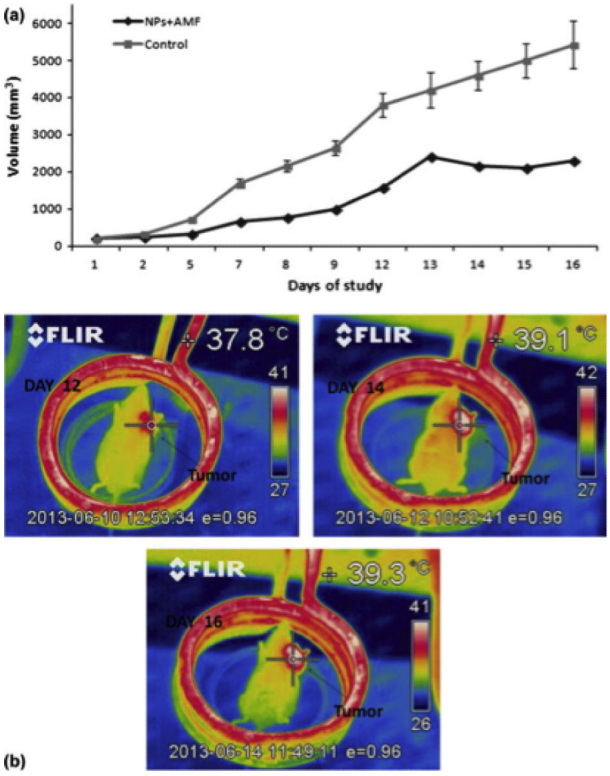


**Fig. 5.**

(a) Tumor volume of a mouse treated with nanoparticles and applied magnetic field and a control group of mice (n = 3) without AMF or nanoparticle injection over an experimental period of 16 days. (b) Thermal images of mouse demonstrated increasing temperatures in the tumor area during hyperthermia sessions in different days of the experimental period. Reproduced with permission from[140], Copyright 2014 Elsevier

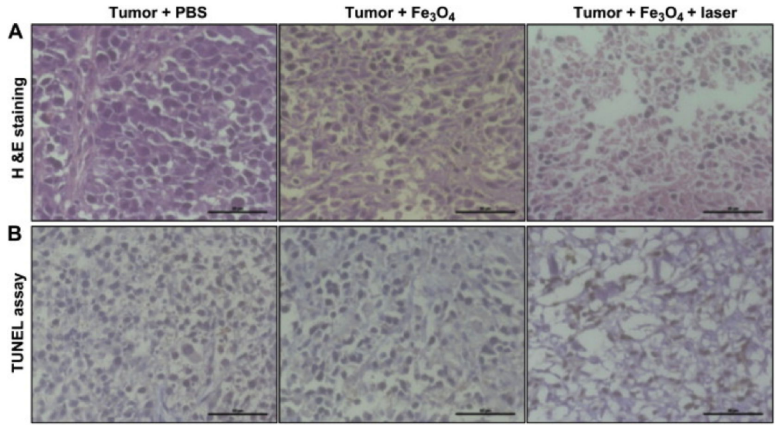


**Fig. 6.**

Histologic assessments of tumor tissues with and without photothermal treatments of $Fe_3O_4$/(DSPE-PEG-COOH) nanoparticles and control. (A) Hematoxylin and eosin (H&E) stained images; (B) terminal deoxynucleotidyl transferase nick end labeling (TUNEL) assay images. The tumor tissues were collected from PBS without laser exposure (left), $Fe_3O_4$/(DSPE-PEG-COOH) without laser exposure (middle), and $Fe_3O_4$/(DSPE-PEGCOOH) with 808-nm laser exposure (right). Scale bar: 50 $\mu$m. Reproduced with permission from[146], Copyright 2013 Elsevier